Thymine as a melt-soluble nucleating agent for poly(3-hydroxybutyrate-*co*-4-hydroxybutyrate)

Hannelore Geeraert [a,b], *Milan Den Haese* [c], *Louis M. Pitet* [c], *Eveline Peeters* [b], *Niko Van den Brande* [a],*

[a] Lab of Physical Chemistry and Polymer Science (FYSC), Research Group of Sustainable Materials Engineering (SUME), Vrije Universiteit Brussel, Pleinlaan 2, 1050 Brussels, Belgium

[b] Research Group of Microbiology (MICR), Vrije Universiteit Brussel, Pleinlaan 2, 1050 Brussels, Belgium

[c] Advanced Functional Polymers (AFP) Laboratory, Institute for Materials Research (imo-imomec), Materials Chemistry Department, Hasselt University, Martelarenlaan 42, 3500 Hasselt, Belgium

[*] Corresponding author

KEYWORDS

Polyhydroxyalkanoate (PHA); Poly(3-hydroxybutyrate-*co*-4-hydroxybutyrate) (P(3HB-*co*-4HB)); Thymine; Biosynthesis; Nucleating agent; Differential Scanning Calorimetry (DSC); Crystallization

ABSTRACT

Poly(3-hydroxybutyrate-*co*-4-hydroxybutyrate) (P(3HB-*co*-4HB)) is a biopolymer with promising biomedical and sustainable material applications, but its slow crystallization complicates processing. In this study, the potential of thymine as a biocompatible nucleating agent was evaluated using polarized optical microscopy (POM), differential scanning calorimetry (DSC), and tensile testing. Poly(3-hydroxybutyrate) (PHB) and P(3HB-*co*-4HB) with 6, 7, and 9 mol% 4HB were biosynthesized in-house using *Cupriavidus* sp. USMAA2-4, ensuring high purity, necessary for this study. Thymine was found to dissolve in the polymer melt and recrystallize into needle-like crystals upon cooling, thereby creating effective nucleation sites. Addition of 1 wt% thymine consistently enhanced the crystallization rate under both non-isothermal and isothermal conditions, although it did not exceed the polymers' intrinsic self-nucleation potential. Initial tensile testing on heat-pressed films further revealed improved ductility in thymine-nucleated samples. These findings highlight the potential of thymine as a melt-soluble additive for enhancing crystallization and mechanical performance of P(3HB-*co*-4HB).

1. Introduction

In the search for sustainable materials, polyhydroxyalkanoates (PHAs) have emerged as a promising family of biobased, biodegradable and biocompatible polymers, synthesized by various microorganisms. With more than 150 different hydroxyalkanoate monomers discovered to date, this group of biopolyesters displays a broad structural diversity, giving rise to versatile material properties [1]. Therefore, application of PHAs is envisaged across various sectors, encompassing packaging, agricultural, and biotechnological industries [2]. Poly(3-hydroxybutyrate) (PHB) is the most commonly synthesized and best-studied member of the PHA family. Among the limited range of PHAs produced on a commercial scale, PHB also currently possesses the highest production capacity [1]. Nonetheless, PHB has certain disadvantages, including a narrow processing window caused by the limited temperature range between its melting point and thermal degradation [1,3]. Additionally, its inherent low nucleation density results in low crystallization rates and the formation of exceptionally large spherulites, on the order of a millimeter in size [4–6]. In addition, secondary crystallization proceeds slowly during storage at room temperature, leading to interspherulitic cracking. These processes contribute to the brittle nature of PHB, which severely limits its application potential [5,6].

Copolymerization of 3-hydroxybutyrate with other hydroxyalkanoate monomers has proven to be an effective strategy to improve the thermomechanical and processing properties of PHB [3]. Among these copolymers, poly(3-hydroxybutyrate-*co*-4-hydroxybutyrate) (P(3HB-*co*-4HB)) holds immense potential for various applications, including high value-added medical and pharmaceutical applications [7]. Increasing the 4-hydroxybutyrate (4HB) content in the copolymer substantially reduces crystallinity and melting temperature, resulting in decreased brittleness, increased elongation at break, and an increased processing window [8]. Unfortunately, even more than PHB, P(3HB-*co*-4HB) exhibits very slow crystallization, posing challenges during processing (e.g., during injection molding) [8]. Improving and

controlling the crystallization behavior of P(3HB-*co*-4HB) is thus of great scientific and industrial interest [9].

Nucleating agents (NAs) play a key role in accelerating crystallization kinetics of semi-crystalline polymers. Incorporation of NAs in the polymer matrix can significantly enhance the nucleation density and thereby crystallization rate. In addition, NAs can improve other properties, including thermal stability and mechanical properties [8,9]. Many different NAs have been investigated to enhance PHB crystallization [10]. In contrast, studies on NAs for P(3HB-*co*-4HB) are more limited. Furthermore, among the NAs reported for P(3HB-*co*-4HB), which include boron nitride [3,11], talc, hydroxyapatite, zinc stearate [11], nano-ZnO [8], silica [12], orotic acid [13], and uracil [14], not every additive holds the same application potential. While boron nitride, for example, is not suitable for human contact applications, orotic acid shows promise as an additive for biomedical applications such as implants, owing to its biodegradable and nontoxic properties [13]. There is a great interest in enhancing the crystallization behavior of P(3HB-*co*-4HB) without compromising its biodegradability and biocompatibility [7,15,16]. Thymine, one of the four DNA nucleobases, has been reported as an efficient biodegradable and biocompatible additive to accelerate PHB [10,17,18], poly(3-hydroxybutyrate-*co*-3-hydroxyvalerate) (P(3HB-*co*-3HV)) [17], and poly(3-hydroxybutyrate-*co*-3-hydroxyhexanoate) (P(3HB-*co*-3HHx)) [18] crystallization. However, the effect of thymine on the crystallization rate of P(3HB-*co*-4HB) has never been reported to the best of our knowledge.

In contrast to externally added nucleating agents (NAs), crystallization can also be strongly enhanced through the persisting "memory" of the polymer's previous crystalline state. When semi-crystalline materials are not processed at sufficiently high temperatures or for long enough times, incompletely melted crystallites (self-seeds) or residual molecular order in the melt (self-nuclei) may remain. Both can act as highly efficient nucleation sites and significantly increase crystallization rates [19]. While self-seeds are considered a type of heterogeneous

nucleation, self-nuclei are described as a special case of homogeneous nucleation [19,20]. The self-nucleation of semi-crystalline polymers offers a useful method to quantify and compare the nucleating efficiency of nucleating agents [21]. Only a limited number of studies have investigated and reported the influence of self-nucleation on the crystallization behavior of PHB and P(3HB-*co*-4HB) [10,22–24].

In this study, we investigate the potential of thymine as a biocompatible nucleating agent for P(3HB-*co*-4HB). The purity and properties of commercial PHAs are often significantly influenced by industrial recovery and processing methods, including the use of (undisclosed) additives such as plasticizers, stabilizers, and nucleating agents [1,25–27]. Furthermore, although research-grade P(3HB-*co*-4HB) copolymers are commercially available, the number of distinct monomer compositions on the market remains limited [1]. To address this, PHB and P(3HB-*co*-4HB) with 6, 7, and 9 mol% 4HB were biosynthesized through cultivation of *Cupriavidus* sp. USMAA2-4 on various carbon sources. To assess the influence of thymine, PHA films with varying thymine concentrations were prepared and subjected to a comprehensive thermal and morphological analysis, including differential scanning calorimetry (DSC), thermogravimetric analysis (TGA), polarized optical microscopy (POM), and tensile testing. Special emphasis was placed on the investigation of non-isothermal and isothermal crystallization kinetics, as well as the nucleating efficiency through application of the DSC self-nucleation protocol. The findings of this study aim to support the development of more efficient and sustainable biopolymers.

2. Materials and methods

2.1 PHA biosynthesis

The polyhydroxyalkanoate (PHA) biosynthesis method employed in this study was derived from the methodology outlined in a publication by Iqbal and Amirul [28]. *Cupriavidus* sp.

USMAA2-4 (DSM 19379) was obtained from DSMZ. The culture stock was stored at -80 °C in 50% (v/v) glycerol. For inoculum preparation, 30 mL of LB medium was inoculated and cultivated at 30 °C and 200 rpm for approximately 18 h. A volume of 5 mL of precultured cells was transferred together with 10 mL of sterile distilled water to a 15 mL falcon tube and centrifuged (Sorvall ST 8R centrifuge, Thermo Fisher Scientific) at 5000 × *g* for 5 min with slow deceleration. The supernatant was discarded, sterile distilled water was added to a total volume of 15 mL, and the precultured cells were centrifuged again under the same conditions. Supernatant was discarded and the washed precultured cells were transferred into 200 mL mineral salts medium (MSM) with the following composition (based on [28]): $K_2HPO_4 \cdot 3H_2O$ (8.0 g/L), KH_2PO_4 (3.7 g/L), $(NH_4)_2SO_4$ (1.1 g/L), $MgSO_4$ (0.3 g/L), and microelement solution (2 mL/L). The microelement solution was composed of $FeSO_4 \cdot 7H_2O$ (2.78 g/L), $MnCl_2 \cdot 4H_2O$ (1.98 g/L), $CoSO_4 \cdot 7H_2O$ (2.81 g/L), $CaCl_2$ (1.26 g/L), $CuCl_2 \cdot 2H_2O$ (0.17 g/L), and $ZnSO_4 \cdot 7H_2O$ (0.29 g/L), in 0.1 mol/L of HCl. The MSM was supplemented by selected carbon source(s) with the total carbon concentration fixed at 0.68 wt% carbon (or C/N ratio equal to 30). Four (combinations of) carbon sources were used: D-fructose (FRU) at 17 g/L; a 1:1 mixture of D-fructose and γ-butyrolactone (FRU + GBL) at 8.8 and 6.3 g/L, respectively; γ-butyrolactone (GBL) at 12.5 g/L; and a 1:1 mixture of D-fructose and 1,4-butanediol (FRU + BDO) at 8.8 and 6.6 g/L, respectively. The pH of each medium was adjusted to 6.90 ± 0.05 by addition of various volumes of a 10 mol/L NaOH solution. All media were cultivated in biological triplicate. Cultivation was performed for 68 hours at 32 °C and 200 rpm. The total experiment (cultivation in biological triplicate in four different media) was repeated three times.

2.2 PHA extraction

After cultivation, the biomass was harvested by centrifugation (Sorvall ST 8R centrifuge, Thermo Fisher Scientific) in 50 mL Falcon tubes at 12108 × *g* for 20 min at 4 °C with slow

deceleration. Biomass pellets were lyophilized (Freezone 71020 Benchtop Freeze Dryer, Labconco) and the weight of the lyophilized biomass was measured, from which the cell dry weight (CDW) concentration was determined as the ratio of the dry biomass weight to the medium volume. Thereafter, the lyophilized biomass was shaken in 50 mL of chloroform for 24 h at 30 °C. Vacuum filtration was performed to remove the cell debris from the extracted PHA using filter paper circles (597 diameter 90 mm, Whatman), followed by normal filtration using folded filter papers (595 ½ diameter 125 mm, Schleicher & Schuell). The extract was concentrated using a rotary evaporator (Rotavapor-R, Büchi) and precipitated under gentle stirring in 75 mL cold ethanol (0-5 °C). The obtained PHA was recovered, left to dry at room temperature for at least two days and then weighed, from which the PHA concentration was determined as ratio of the PHA weight to the medium volume.

2.3 Structural characterization

Chemical structure and composition of the biosynthesized PHAs were determined using proton nuclear magnetic resonance (^{1}H NMR) spectroscopy. PHA samples were dissolved in deuterated chloroform ($CDCl_3$, containing 0.03 % (v/v) tetramethylsilane (TMS)) at 4 mg/mL under magnetic stirring at 55 °C for one hour, after which approximately 0.7 mL was transferred to an NMR tube. ^{1}H NMR spectra were recorded using a Bruker AscentTM 400 magnet equipped with an Avance NEO console and HR-BBO iProbe operating at 400.20 MHz. Spectra were recorded at 300 K using standard Bruker pulse programs, with a relaxation delay (D1) of 20 s. Data were processed in TOPSPIN v4.1.4 from Bruker Biospin.

Size exclusion chromatography (SEC) was used to study the molar mass (distribution) of the biosynthesized PHAs. Samples were dissolved in purified chloroform ($CHCl_3$, with 100 ppm toluene as internal standard) at 5.0 ± 0.1 mg/mL and filtered using a 0.45 PTFE syringe filter. 100 µL was passed through a SEC system (HLC-8320GPC EcoSEC, Tosoh Bioscience) at 1

mL/min with a column set consisting of a PSS SDV (5 µm particle size) precolumn (50 x 8 mm) and two PSS SDV analytical linear M columns (300 x 8 mm). The system was equipped with a multi-angle laser light scattering detector (MALS, $LenS_3$ (TOSOH)) and a refractive index detector (Bryce-type differential refractometer (RI), ECOSEC Elite HLC-8420GPC). Data acquisition and processing was carried out using SECView software (Tosoh Bioscience). Determination of the weight-average molar mass (M_w) and dispersity ($Đ$) of all biosynthesized samples solely from the RI signal was based on calibration by polystyrene standards (Polymer Standards Service; PSS) with a molar mass ranging from 0.4 – 1000 kDa. Determination of M_w and $Đ$ by the MALS detection system was based on hydrodynamic volume of the solute via specific refractive index increment, with *dn/dc* values calculated from the PHA concentration, assuming a 100% quantitative recovery of the samples.

2.4 Preparation of reference and thymine-nucleated PHA films

Thymine powder (≥ 99%) with a melting temperature of 320 °C was purchased from Sigma-Aldrich Co., Ltd. (Shanghai, China) and used as received. As described above, cultivation was performed in biological triplicate for each of the four media, with three independent repetitions of the entire cultivation experiment. For the preparation of the PHA films, equal amounts of the nine subsamples of biosynthesized PHA from each medium were mixed, ensuring sufficient material and a representative sample that captures the variability within each cultivation condition. Two film variants, differing in average film thickness, were prepared for different experimental purposes: variant A (~35 µm) and variant B (~100 µm).

Variant A films were prepared by dissolving 300 mg of PHA in 20 mL of chloroform at 55 °C under magnetic stirring for 40 min. During this time, the desired amount of thymine (0, 1.5 ± 0.1, 3.0 ± 0.1, and 6.0 ± 0.1 mg, corresponding to 0 (reference), 0.5, 1, and 2 wt% films, respectively) was weighed and suspended in 10 mL of chloroform. The thymine suspension

was ultrasonicated for 40 min at room temperature and added to the PHA solution, which was then mixing at 55 °C under magnetic stirring for 24 h. The mixture was cast in a glass Petri dish (⌀ 100 mm) and left for solvent evaporation and drying for at least 7 days before characterization. A reference film was prepared for each of the four cultivation media. For the FRU + GBL medium, a films with 0.5, 1, and 2 wt% thymine were prepared. For the other media, a film with 1 wt% thymine was prepared.

Variant B films were prepared following the same method outlined above, with the following adjustments: solvent casting was performed in smaller crystallization dishes (⌀ 60 mm) to obtain increased film thickness, and the films were left for at least 14 days before characterization. A reference and a film with 1 wt% thymine were prepared for each cultivation medium tested.

2.5 Thermogravimetric analysis (TGA)

The thermal stability of reference and 1 wt% thymine-nucleated PHA films (variant A) was studied by TGA (TGA Q5000, TA instruments). For each sample, 2.0 ± 0.2 mg was placed in a 100 µL platinum pan. The temperature was first stabilized at 50 °C, and then increased at 10 K/min to 600 °C, all under a nitrogen flow rate of 25 mL/min. TGA analysis was repeated three times for each (reference or thymine-nucleated) PHA film, and the average temperatures at which 2, 5, and 10 % of the weight was lost ($T_{2\%}$, $T_{5\%}$, and $T_{10\%}$, respectively), as well as the average temperature at which the rate of thermal decomposition was the highest ($T_{d,max}$), were determined.

2.6 Differential scanning calorimetry (DSC)

The thermal properties and crystallization behavior of reference and thymine-nucleated PHA films were studied by DSC (DSC Discovery; TA Instruments). For each sample, 3.0 ± 0.2 mg

was loaded into a aluminum T-zero hermetic DSC pan (TA instruments). All experiments were conducted under a nitrogen flow of 50 mL/min. The samples were subjected to the thermal protocols described below.

Quenching The sample was heated from 30 °C to 200 °C at 10 K/min, held isothermal for 3 min at 200 °C, cooled to -50 °C at 40 K/min, held isothermally for 1 min at -50 °C, and reheated to 200 °C at 10 K/min. From this analysis, the glass transition temperature (T_g) was determined as the midpoint of the characteristic change in the baseline of the heat flow curve during the second heating step. For each reference PHA film (variant A), two replicate measurements were performed, and the average T_g was determined.

Non-isothermal crystallization The sample was heated from 30 °C to 200 °C at 10 K/min, held isothermal for 3 min at 200 °C, cooled to -50 °C at the desired cooling rate (5 or 10 K/min), held isothermal for 1 min at -50 °C, and reheated to 200 °C at 10 K/min. From the cooling step, the melt-crystallization temperature (T_{mc}) was determined at the minimum of the exothermic peak in the heat flow curve, and the corresponding melt-crystallization enthalpy (ΔH_{mc}) by integrating the area under this exothermic peak. The cold-crystallization temperature (T_{cc}) was determined at the minimum of the exothermic peak observed during the subsequent heating step. The melting enthalpy (ΔH_m) was determined by integrating the area under the endothermic melting peak observed, also during the second heating step. The degree of crystallinity (X_c) was then estimated as the ratio of ΔH_m and ΔH_m^0 (146 J/g [29]), the melting enthalpy of 100 % crystalline PHB, and corrected for the weight fraction of nucleation agent (α):

$$X_c = 100\ \% \cdot \frac{\Delta H_m \cdot (1+\alpha)}{\Delta H_m^0} \qquad (1)$$

This thermal protocol was applied to all reference and thymine-nucleated PHA films of variant A. For each combination of film and cooling rate, two replicate measurements were performed, and the average T_{mc}, ΔH_{mc}, T_{cc}, ΔH_m, and X_c were determined.

Isothermal crystallization The sample was heated from 30 °C to 200 °C at 10 K/min, held isothermal for 3 min at 200 °C, cooled at 40 K/min to the desired isothermal crystallization temperature (T_c) and maintained at this temperature for 60 to 600 min, to ensure complete crystallization. Then, the sample was further cooled to -50 °C at 10 K/min, held isothermal for 1 min at -50 °C, and reheated to 200 °C at 10 K/min. To account for the transient overshoot signal, produced when switching from the cooling to the isothermal step (at the crystallization temperature), a blank run was performed on one sample for each (reference or 1 wt% thymine-nucleated) PHA film (variant A). The method for this blank run was identical to the isothermal crystallization protocol just described, but with the isothermal step performed at 170 °C for 30 min, since no crystallization is expected to occur at these conditions. The isothermal crystallization exotherms and the blank runs were vertically shifted to yield an average heat flow rate of zero at the end of the isothermal step. After subtraction of the blank run from the isothermal crystallization exotherm, the onset time of crystallization (τ_0) was determined and the relative crystallinity X_{rel} at time t, measured from τ_0, was calculated. From X_{rel} as a function of t, the crystallization half-time ($\tau_{0.5}$) was determined and the isothermal crystallization kinetics were analyzed through the Avrami equation. When samples displayed irregularly shaped crystallization exotherms at certain crystallization temperatures, a replicate measurement was made and the average $\tau_{0.5}$ and Avrami parameters were determined.

Self-nucleation At a rate of 10 K/min, the sample was heated from 30 °C to a self-nucleation temperature (T_s), held isothermal for 3 min at T_s, cooled to -50 °C at 10 K/min, held isothermal for 1 min at -50 °C, and reheated to 200 °C at 10 K/min. From the cooling step, the melt-crystallization temperature (T_{mc}) was determined at the minimum of the exothermic peak in the heat flow curve. This thermal protocol was applied to each reference PHA film (variant A).

2.7 Polarized optical microscopy (POM)

Non-isothermal The morphology and dispersion of thymine in 1 wt % thymine-nucleated PHA films (variant B) during non-isothermal crystallization were observed using a polarized optical microscope (POM; MT9930L, Meiji Techno) in transmitted light mode, equipped with a temperature control stage (CI94 temperature controller with LTS350 microscope stage and LNP95 liquid nitrogen cooling system, Linkam). Circular samples (⌀ 5 mm) were placed on a glass slide, covered by a circular coverslip (⌀ 9 mm). Samples were heated to 200 °C at 10 K/min, held isothermal for 3 min, and cooled at 10 K/min until crystallization was complete. Images were captured every 10 °C using a HD1500 camera (Meiji Techno).

Isothermal The spherulite growth rate during isothermal crystallization was examined using the same POM setup. Circular samples (⌀ 9 mm) were placed on a glass slide, covered by a coverslip. Samples were heated to 200 °C at 30 K/min, and held isothermal for 3 min, during which, only for the thymine-nucleated samples, the coverslip was gently pressed down using tweezers to reduce the film thickness. Thereafter the sample was cooled at 30 K/min (the maximum cooling rate of the instrument) to the isothermal crystallization temperature. Videos were captured during crystallization, from which screenshots were made every 2 to 20 s (depending on the growth rate), and the spherulite radius was measured for every screenshot. The growth rate was determined by plotting the spherulite radius as a function of time and obtaining the slope of the linear regression of the datapoints. For each reference and 1 wt% thymine-nucleated PHA film (variant A), five samples were studied, and from every sample the spherulite growth rate of one to five spherulites was determined. The spherulite growth rate was reported as the average (± standard deviation) of all spherulites studied for PHA film.

2.8 Tensile testing

After preparation of the reference and thymine-nucleated PHA films (variant B), they were left to age for 14 days, after which three tensile test specimens were cut from each film and tested, with results averaged. The remaining portions of the films were then heat-pressed using a hydraulic laboratory press (LabManual 50, Fontijne Presses). Each reference film and its corresponding thymine-nucleated film were placed side by side in a steel mold with ± 0.1 mm spacing, and heat-pressed for 3 minutes at 200 °C. Following pressing, the mold was left between the plates with the press turned off to allow passive cooling to room temperature. Tensile testing of the heat-pressed films was conducted after 14 days of aging (five samples, results averaged).

All tensile tests were performed at room temperature using a TA Instruments DMA Q800 equipped with a film tension clamp. For each test, a 20 mm × 3 mm (length x width) rectangular sample was cut from the film and clamped with a gauge length of 8-10 mm. Data was collected at a strain rate of 50 %/min. The elastic modulus was obtained by measuring the slope in the linear region of the stress-strain curve. To correct for initial strain offset, stress–strain data were horizontally shifted so that the extrapolated linear region passed through the origin. The tensile strength was determined as the maximum stress measured during the test, while the elongation at break was recorded as the strain at the point of failure. The solvent-cast and heat-pressed samples were imaged using a polarized optical microscope (ZEISS Axioscope 5) equipped with 0.15 pol n-achroplan objectives. Images were captured using Zen3.1 blue.

3. Results and discussion

3.1 PHB and P(3HB-co-4HB) biosynthesis

PHB and P(3HB-*co*-4HB) polymers were produced by *Cupriavidus* sp. USMAA2-4 cultures in a shake-flask setup. Samples with varying composition and molar mass were produced by

altering the carbon source(s) supplied in the medium, while maintaining a constant total carbon concentration and C/N ratio. Each cultivation experiment was performed in biological triplicate to account for variability within the biological system. Additionally, the entire cultivation experiment was repeated three times to assess the reproducibility of the results and minimize technical variability. As a result, nine subsamples were synthesized for each medium. The average CDW concentration and PHA concentration are presented in Table 1. The composition, molar mass, and dispersity of each subsample were determined using ^{1}H NMR spectroscopy and SEC, respectively. Figure S1 (Supporting Information) shows a representative ^{1}H NMR spectrum of a P(3HB-*co*-4HB) material. The signals corresponding to position 3 of the 3HB monomer unit and position 4 of the 4HB monomer unit (chemical shifts at 5.3 and 4.1 ppm, respectively), were individually resolved. The fraction of 4HB units in the copolymer P(3HB-*co*-4HB) was determined by integrating the signal intensity of these proton signals in the ^{1}H NMR spectra. The average structural characterization results for each medium are presented in Table 1.

Cultivation of *Cupriavidus* sp. USMAA2-4 on different (combinations of) carbon sources resulted in only slight variations in P(3HB-*co*-4HB) composition (Table 1). PHA metabolism consists of dynamic, bidirectional processes involving both synthesis and degradation, and is intricately connected to the central metabolic network [28]. Consequently, environmental parameters significantly influence PHA accumulation. This complexity makes direct comparisons with previously reported PHA synthesis by *Cupriavidus* sp. USMAA2-4 challenging, as experimental parameters are often not identical. Although many of the experimental parameters in this study - including the composition of the MSM, pH, C/N ratio, nitrogen source, total carbon concentration, and incubation temperature – were based on the study by Iqbal and Amirul [28], substantial differences in PHA accumulation were observed compared to their results. For instance, in cultivation using γ-butyrolactone (GBL) as the sole

carbon source, a higher overall PHA concentration was achieved in this study (2.2 g/L, Table 1) compared to the values reported by Iqbal and Amirul (1.3 or 1.7 g/L) [28]. However, the 4HB composition was significantly lower (7.0 mol% in Table 1 versus 36 or 34 mol% in [28]). These differences are most likely due to variations in other experimental parameters such as incubation time, culture volume, or inoculation method. Among other factors, initial cell concentration has been shown to strongly influence both PHA accumulation and composition, as demonstrated by Vigneswari et al. [30] for P(3HB-*co*-4HB) synthesis by cultivation of *Cupriavidus* sp. USMAA1020 cultivated on GBL.

While the weight-average molar mass (M_w) and dispersity ($Đ$) of the PHA materials obtained from cultivation on media containing D-fructose (FRU) were quite similar, lower M_w and $Đ$ values were observed when GBL was used as the sole carbon source (Table 1). All other culture conditions, including the C/N ratio, incubation time, and initial pH, were kept constant. The influence of the carbon source on PHA metabolism - and consequently on the resulting PHA molar mass - has been reported in the literature [31,32]. Iqbal and Amirul [28] observed that the molar mass of P(3HB-*co*-4HB) copolymers produced by *Cupriavidus* sp. USMAA2-4 was lower when cultivated on media with high concentrations of 4HB precursors, compared to those grown on media with high concentrations of oleic acid. This is consistent with the findings of the present study, as GBL, unlike FRU, is a 4HB precursor.

Even though different samples of the same polymer can be objectively compared, it is important to note that M_w determined via RI is based on polystyrene standards and may deviate from the true molar mass due to differences in polymer-solvent interactions. MALS, by contrast, provides an absolute molar mass measurement based on laser scattering as a function of hydrodynamic volume. In this method, the intensity of the scattered light (R_θ) is correlated with molar mass using the Rayleigh equation. When comparing $Đ$ values, RI-based calculations provided accurate data due to the high signal-to-noise ratio (Table 1), in contrast

to the values obtained from MALS, which tend to be less reliable (Supporting Information, Table S1).

Table 1. CDW, PHA concentration, and structural characterization of PHA produced by *Cupriavidus* sp. USMAA2-4 cultivated on different carbon sources.

Carbon source(s)	CDW (g/L)	PHA (g/L)	4HB (mol%)	Mw by MALS (kg/mol)	Mw by RI (kg/mol)	Đ by RI (-)	Sample name
FRU	7.1 ± 0.8	0.8 ± 0.3	0.0 ± 0.0	416.4 ± 9.2	624 ± 15	1.9 ± 0.1	PHB
FRU + GBL	6.2 ± 0.9	1.9 ± 0.2	5.9 ± 0.6	440 ± 23	611 ± 17	1.7 ± 0.1	P34HB-6%
GBL	6.0 ± 1.1	2.2 ± 0.3	7.0 ± 1.2	310 ± 13	427 ± 19	2.5 ± 0.2	P34HB-7%
FRU + BDO	6.8 ± 0.5	2.2 ± 0.1	8.9 ± 1.2	407 ± 13	607 ± 20	1.8 ± 0.2	P34HB-9%

All results are the average (± standard deviation) from three experiments, each performed in biological triplicate.

3.2 Thermal characterization of PHB and P(3HB-co-4HB) reference films

For each of the four PHA materials resulting from cultivation on different (combinations of) carbon sources, a reference films was prepared. The films were labeled according to the samples names presented in Table 1, reflecting the average PHA composition of each sample. Prior to studying the influence of thymine on PHB and P(3HB-co-4HB), thermal characterization of the reference films was performed.

The DSC quenching protocol was applied to characterize the glass transition temperature (T_g) of the materials, with results summarized in Table 2. T_g was found to decrease with increasing 4HB content in the copolymer, consistent with observations made in other studies [6,33]. This trend is commonly attributed to increased flexibility of the polymer backbone [34,35].

The melting behavior of PHB and P(3HB-co-4HB) was studied using the DSC non-isothermal crystallization protocol with a cooling rate of 10 K/min. The first cooling and second

heating steps of the DSC thermograms from one repetition are shown in Figure 3 (dashed lines). Melting temperatures (T_m), defined by peak maxima, were recorded during the second heating step. Multiple melting peaks were observed for all samples. Although alternative explanations cannot be excluded, this behavior is most likely due to the melting-recrystallization-remelting phenomenon commonly observed in PHAs [6,36,37]. All identifiable peak maxima are summarized in Table 2. In agreement with literature, T_m decreased with increasing 4HB content [6,33,38]. However, a small deviation from this trend was observed for P34HB-7%, which exhibited a second melting peak at 147 °C – lower than that of P34HB-9% (152 °C). This deviation can be attributed to the lower molar mass of P34HB-7% (Table 1), which is known to depress the melting temperature [34].

The melting enthalpy (ΔH_m) of the PHB and P(3HB-co-4HB) reference films was measured during the second heating step (Table 3). The degree of crystallinity (X_c) was estimated from the ratio of ΔH_m to the melting enthalpy of 100 % crystalline PHB (ΔH_m^0= 146 J/g [29]), and also reported in Table 3. As the 4HB content increased, ΔH_m and X_c decreased. It is known that the lattice parameters of P(3HB-co-4HB) do not change with increasing 4HB content, suggesting that 4HB monomers are not incorporated into the 3HB crystalline lattice. Since no co-crystallization occurs, 4HB units act as defects, reducing the degree of crystallinity [6,35,39].

Table 2. Thermal properties of reference PHB and P(3HB-*co*-4HB) films.

Sample	T_g (°C)[a]	T_m (°C)[b]
PHB	-1	166
P34HB-6%	-4	134, 162
P34HB-7%	-4	126, 147
P34HB-9%	-6	123, 152

[a] Determined using DSC analysis: quenching; [b] Determined using DSC analysis: non-isothermal crystallization (10 K/min cooling rate) from second heating step. In case multiple melting peaks were observed, all identifiable peak maxima are reported as melting temperature (T_m).

3.3 Nucleation behavior of P34HB-6% on thymine during non-isothermal crystallization

To gain initial insight into the effect of thymine on the nucleation behavior of the polymer, polarized optical microscopy (POM) was first applied to P34HB-6% with 1 wt% thymine (labeled P34HB-6%/TM1). By starting with a single polymer-additive combination, the fundamental interaction between thymine and the polymer matrix could be explored before extending the investigation to other compositions. The sample was subjected to a non-isothermal crystallization protocol consisting of heating to 200 °C at 10 K/min, an isothermal hold for 3 minutes, and cooling at 10 K/min. POM images captured at various temperatures throughout the thermal protocol are shown in Figure 1.

Although processed far below the melting temperature of thymine (316 ºC [40]), POM revealed that thymine does not remain solid during "melt processing". In fact, thymine crystals, initially visible as birefringent particles during heating (Figure 1a and b), appear to gradually dissolve in the polymer melt. After the 3 min isothermal hold at 200 ºC, almost complete dissolution is observed (Figure 1c). Upon cooling of the polymer melt, thymine recrystallizes in the form of needle-like crystals, ranging in length from a few hundred micrometers to several millimeters (Figure 1d). These recrystallized thymine structures then provide crystalline surfaces that facilitate heterogeneous nucleation of the polymer during recrystallization (Figure 1e and f). Ma et al. [10] proposed that epitaxial nucleation is the mechanism by which thymine enhances crystallization in PHB, based on a near-perfect lattice match between the PHB and thymine crystal structures. Since 4HB monomers are not incorporated into the 3HB crystalline lattice, the same mechanism is expected to occur in the P(3HB-co-4HB) system.

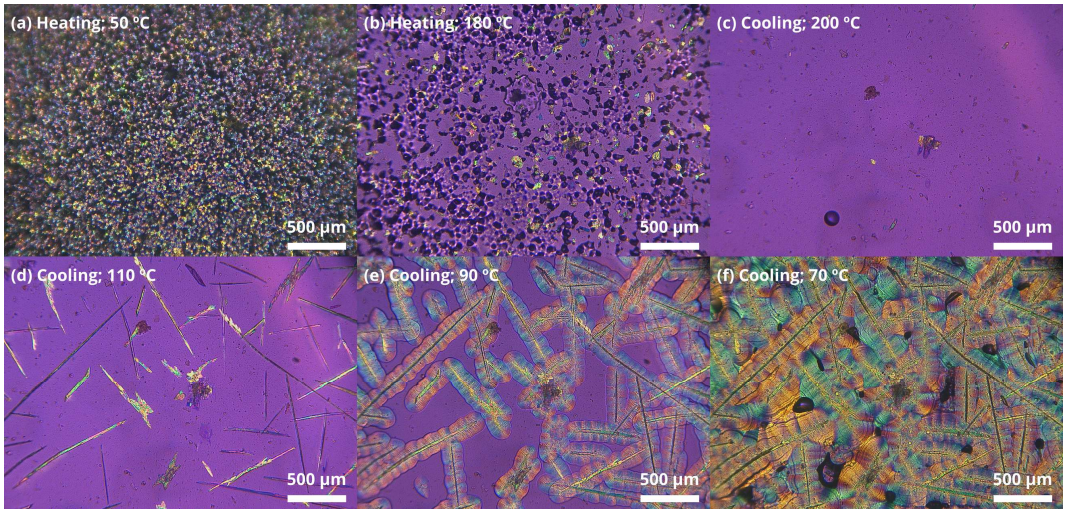

Figure 1. Observation of thymine dissolution and recrystallization as needle-like crystals in P34HB-6%/TM1 using polarized optical microscopy (POM). Images were taken during heating (10 K/min) to 200 ºC at (a) 50 ºC and (b) 180 ºC, (c) at the end of the 3 min isothermal hold at 200 ºC, and during the subsequent cooling phase (10 K/min) at (d) 110 ºC, (e) 90 ºC, and (f) 70 ºC.

This study is, to the best of our knowledge, the first to demonstrate the (partial) solubility of thymine in a polymer melt, although thymine has previously been reported as a nucleating agent for various PHAs [10,17,18], and other polymers. Although thymine has a high melting point (~ 316 °C), it dissolves in P34HB-6% at 200 °C, enabled by strong polymer–additive interactions, especially hydrogen bonding interactions, causing melting point depression [41]. Similar behavior has been described for other melt-soluble nucleation agents, such as oxalamide compounds in PHA [42] and PLA [43] systems. Shen et al. [43] stated that the PLA matrix behaves as a solvent of the oxalamide molecules due to strong hydrogen-bonding interactions. Although also described for other polymer-additive systems, the dissolution and recrystallization of low concentrations of NAs in the polymer melt often remains undetected, because of the low signal intensity in DSC [43]. Compared to insoluble compounds, thymine is expected to exhibit better dispersibility during (industrial) melt processing, thereby promoting more uniform nucleation [44].

3.4 Effect of varying thymine concentration on non-isothermal crystallization of P34HB-6%

Since POM revealed nucleation of P34HB-6% on thymine crystals, the effect of varying thymine concentration on the non-isothermal crystallization of P34HB-6% was further investigated using DSC. Samples containing 0.5, 1, and 2 wt% thymine, were labeled P34HB-6%/TM05, P34HB-6%/TM1, and P34HB-6%/TM2, respectively. The resulting DSC thermograms (from a single replicate) are shown in Figure 2, while the average thermal parameters are provided in the Supporting Information (Table S2).

For P34HB-6%, P34HB-6%/TM1, and P34HB-6%/TM2, similar trends were observed at both cooling rates. Neat P34HB-6% exhibited partial crystallization during cooling (melt-crystallization) and further crystallization during the subsequent heating step (cold-crystallization). In contrast, samples with 1 and 2 wt% thymine showed only melt-crystallization (Figure 2). Furthermore, the melt-crystallization temperature (T_{mc}) shifted towards higher values (and thus lower supercooling), indicating an increased non-isothermal crystallization rate of P34HB-6% upon thymine addition. The average T_{mc} shift was slightly lower for P34HB-6%/TM2 than for P34HB-6%/TM1 (Table S2). This could be attributed to an excess of thymine reducing the mobility of the polymer chains, thereby hindering crystallization [44,45]. Moreover, higher concentrations may affect the dispersion and aggregation of thymine, which in turn could alter the size and morphology of the thymine crystals formed upon recrystallization, thereby influencing the number of effective nucleation sites [46].

At a cooling rate of 10 K/min, P34HB-6%/TM05 exhibit a peculiar behavior. Instead of the usual two, four replicate DSC runs were performed. Two of these runs showed only cold-crystallization, with a lower cold-crystallization temperature (T_{cc}) compared to neat P34HB-6% (see P34HB-6%/TM05-1 in Figure 2b and Table S2). In contrast, the other two runs showed complete melt-crystallization with a nucleating efficiency between that of the 1 and 2 wt% (see

P34HB-6%/TM05-2 in Figure 2b and Table S2). These inconsistent results obtained for P34HB-6% with 0.5 wt% thymine at a 10 K/min cooling rate are most likely caused by variations in the thymine concentration. In some regions of the solvent-cast film (and thus in some DSC samples), the local thymine concentration may have been too low to allow recrystallization, or thymine recrystallization may have occurred only at temperatures below the polymer's melt-crystallization temperature range during cooling at 10 K/min. As a result, thymine was unable to effectively nucleate P34HB-6% under these conditions (P34HB-6%/TM05-1 in Figure 2b). Even more, the dissolved thymine hindered the melt-crystallization process. For neat P34HB-6%, crystallization occurred partly during cooling and party during the subsequent heating. In contrast, only cold-crystallization was observed for P34HB-6%/TM05-1 (Figure 2b). This behavior is characteristic of (partially) soluble nucleating agents and is often attributed to the dissolved additive in the polymer melt acting as a (poor) solvent, thereby reducing the polymer's crystallization ability [46–48]. This contrasts with insoluble nucleating agents, which typically exhibit nucleation effects even at very low concentrations [44,48]. During the subsequent heating step, cold-crystallization of P34HB-6%/TM05-1 occurred at lower temperatures than for neat P34HB-6% (Figure 2b, Table S2). It is hypothesized that at lower concentrations, thymine also recrystallizes, though at lower temperatures (likely only upon reheating the sample above its T_g), which in turn enhances the cold crystallization of P34HB-6% [46].

At a cooling rate of 5 K/min, complete melt-crystallization was observed for P34HB-6% with 0.5 wt% thymine across all four replicates (Figure 2a). This suggests that, at the slower cooling rate, thymine had sufficient time to recrystallize during cooling. However, in some replicate runs, the shift in T_{mc} was less pronounced, likely due to incomplete thymine recrystallization prior to the onset of the polymer's melt-crystallization. As a result, the average

T_{mc} value for P34HB-6%/TM05 was lower than that of P34HB-6%/TM2 (and P34HB-6%/TM1) at the 5 K/min cooling rate (Table S2).

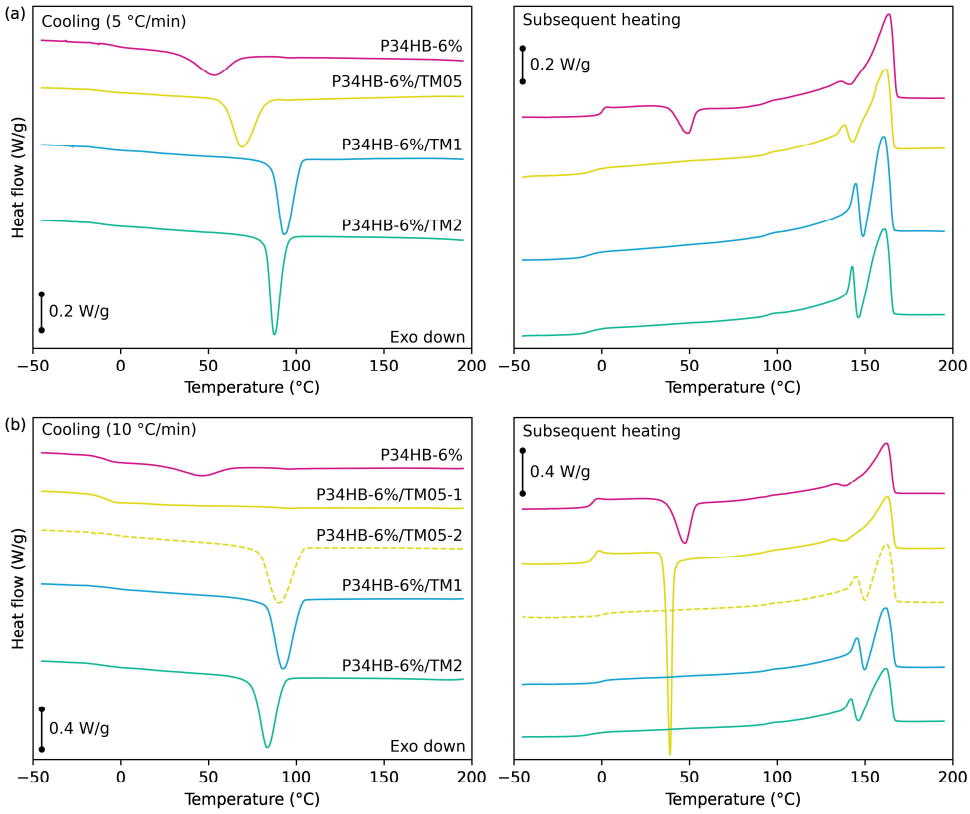

Figure 2. DSC thermograms of non-isothermal crystallization for P34HB-6% and its mixtures with 0.5, 1, and 2 wt% thymine. Both the cooling and subsequent heating steps from a single representative run are shown for cooling rates of (a) 5 K/min and (b) 10 K/min. In (b), two distinct crystallization behaviors for P34HB-6%/TM05 are presented.

In addition to the thymine concentration, dispersion, and thermal conditions during cooling, both the polymer composition and melt processing conditions can significantly influence the thymine recrystallization, including through variations in melt viscosity [44,49]. These factors may also affect the number of effective nucleation sites by altering the size and morphology of the recrystallized thymine crystals [46]. Ma et al. [42] observed that the self-organization of certain oxalamide compounds into large, needle-shaped aggregates occurred at concentrations above

0.5 wt% in PHB and was accompanied by a decrease in nucleating efficiency compared to smaller particles, due to the reduced surface-to-volume ratio. Given that 1 wt% thymine resulted in the greatest (and most consistent) increase in the non-isothermal crystallization rate of P34HB-6%, this concentration was selected to evaluate the nucleating efficiency across all four PHB and P(3HB-*co*-4HB) samples. However, future studies should explore the relationship between thymine dispersion, crystal morphology, and nucleation efficiency in greater detail to better understand and optimize its performance across different polymer systems.

3.5 Nucleating efficiency of thymine during non-isothermal crystallization

PHB, P34HB-7% and P34HB-9% were each solvent-mixed with 1 wt% thymine and labeled PHB/TM1, P34HB-7%/TM1, and P34HB-9%/TM1, respectively. The dissolution and recrystallization of thymine in these materials was investigated by POM (Supporting Information, Figures S2–S4). Comparable dissolution–recrystallization and nucleation behavior was observed across all three materials, consistent with the results obtained for P34HB-6%/TM1 described in Section 3.3.

Thereafter, DSC was applied to evaluate the effect of 1 wt% thymine on the non-isothermal crystallization of PHB, P34HB-7% and P34HB-9%. Representative DSC thermograms recorded at a 10 K/min cooling rate, are presented in Figure 3, with the corresponding average thermal parameters provided in Table 3. Results obtained using a 5 K/min cooling rate are provided in Supporting Information (Figure S5 and Table S3). Data for P34HB-6% are also included for comparison and to provide a comprehensive overview.

For PHB, T_{mc} shifted to higher values after addition of 1 wt% of thymine. In the case of P34HB-7% and P34HB-9% reference films, only cold-crystallization was observed. In contrast, the thymine-nucleated samples, P34HB-7%/TM1 and P34HB-9%/TM1, exhibited only melt-crystallization. These results demonstrate enhanced crystallization rates in all studied

PHB and P(3HB-*co*-4HB) materials after solvent mixing with 1 wt% thymine, under both cooling rates.

Interestingly, similar or only slightly increased degree of crystallinity values (X_c) were observed (Table 3 and Table S3). However, it should be noted that a small enthalpic contribution from the dissolution of thymine, potentially overlapping with the melting endotherm, was not accounted for. Additionally, for materials where a cold crystallization is observed, this may lead to a small error in the determination of the melting enthalpy.

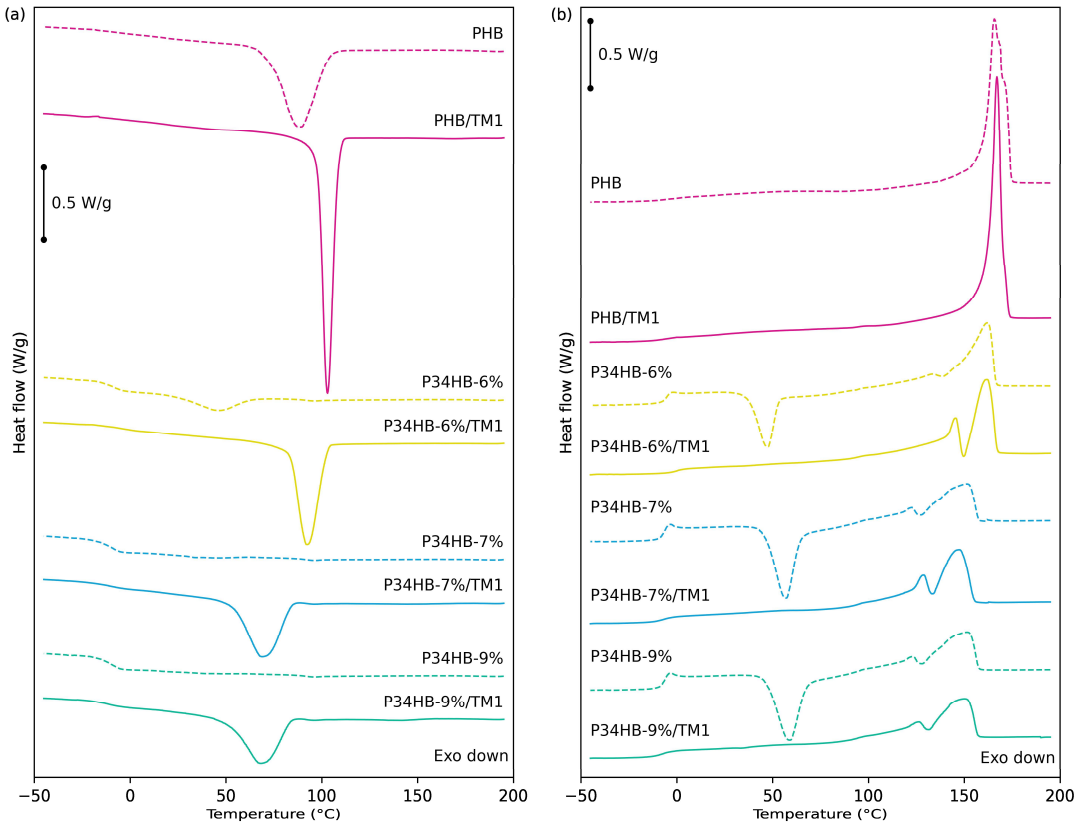

Figure 3. DSC thermograms of non-isothermal crystallization for PHB, P34HB-6%, P34HB-7%, P34HB-9%, and their respective mixtures with 1 wt% thymine. Shown are the (a) cooling (at 10 K/min) and (b) subsequent heating steps from a single representative run for each sample.

Table 3. Crystallization parameters of PHB, P34HB-6%, P34HB-7%, P34HB-9%, and their respective mixtures with 1 wt% thymine, determined by non-isothermal crystallization at a cooling rate of 10 K/min using DSC. Values represent the average of two independent runs.

	Cooling		Subsequent heating		
Sample	T_{mc} (peak) (°C)	ΔH_{mc} (J/g)	T_{cc} (peak) (°C)	ΔH_m (J/g)	X_c (%)
PHB	88	67	-	88	60
PHB/TM1	103	75	-	89	61
P34HB-6%	46	17	48	56	38
P34HB-6%/TM1	91	53	-	60	42
P34HB-7%	-	-	57	51	35
P34HB-7%/TM1	68	45	-	56	39
P34HB-9%	-	-	59	44	30
P34HB-9%/TM1	66	42	-	50	34

To quantify the nucleating efficiency of 1 wt% thymine, its effect should be compared to the self-nucleation potential of the neat PHB and P(3HB-*co*-4HB) reference films [50]. According to standard self-nucleation protocols, a "standard semi-crystalline state" is first established by heating the sample to at least 25-30 °C above its melting temperature, followed by an isothermal step and controlled cooling. Afterwards, the sample can be heated to the self-nucleation temperature (T_s) [19,51,52]. However, for polymers that are sensitive to thermal degradation, such as PHAs, an adapted protocol is recommended. In this approach, the pristine sample is directly heated to T_s, and held isothermally for a short duration (1–5 minutes) to minimize thermal degradation. Furthermore, a fresh DSC sample is prepared for each T_s tested [53,54]. This approach assumes identical pre-treatment procedures for all samples, which is valid for this study. The first cooling and subsequent heating steps of the DSC thermograms,

resulting from application of the adapted self-nucleation protocol, are shown in Figure 4a for P34HB-6%, for selected T_s. The melt-crystallization temperature (T_{mc}), determined from the cooling steps, is plotted as function of T_s in Figure 4b. Corresponding data for PHB, P34HB-7%, and P34HB-9% are presented in the Supporting Information (Figures S6-S8).

Typically, three self-nucleation domains can be distinguished depending on T_s (for a fixed processing time). At high T_s, an isotropic melt is produced and only high-temperature-resistant heterogeneous nuclei remain. This is referred to as domain I (DI). In DI, crystallization becomes reproducible and independent of T_s. When T_s is lowered, domain II (DII) is entered, and memory of the previous crystalline state persists. For PHB (Figure S6) and P34HB-6% (Figure 4), when T_s is decreased below 200 and 188 °C, respectively, the melt-crystallization exotherms shift to higher temperatures with decreasing T_s. This increase in T_{mc} with decreasing T_s is indicative of DII [19]. For the P34HB-7% (Figure S7) and P34HB-9% (Figure S8), a shift towards lower temperatures and/or decreasing intensity of the cold-crystallization peak is observed for T_s below 186 and 184 °C, respectively. In addition to the appearance of a melt-crystallization peak, this behavior suggests a possible transition between DI and DII. For higher T_s in DII (subdomain IIa), crystallization is accelerated only by the presence of self-nuclei. In contrast, for lower T_s (subdomain IIb), additional crystal fragments (self-seeds) remain. The end of the melting endotherm, as observed by DSC during the first heating step, marks the boundary between IIa and IIb, and is indicated by a vertical dashed line in Figure 4b and in Figures S5–S7 [55]. Upon further reduction of T_s, domain III (DIII) is reached, characterized by the appearance of an additional high-temperature peak during the second melting step. This peak indicates that unmolten crystal fragments underwent annealing during the isothermal hold at T_s [19,56]. Each occurrence of this peak is marked with an arrow in Figure 4a and in Figures S6–S8. Moreover, in DIII, the crystallization exotherm is typically broad and may exhibit a double peak, as observed clearly for P34HB-6%, T_s = 160 ºC (Figure 4a) [57–59]. In all cases, T_{mc}

was determined as the temperature at the minimum of the exothermic crystallization signal, corresponding to the most intense crystallization peak.

The ideal self-nucleation temperature ($T_{s,ideal}$) is defined as the temperature that induces the highest melt-crystallization temperature ($T_{mc,max}$), without the presence of annealing in the subsequent heating. In other words, $T_{s,ideal}$ is the lowest T_s within DII [60]. For P34HB-6%, a $T_{s,ideal}$ of 164 °C was identified, resulting in a $T_{mc,max}$ of 107 °C. The values of $T_{s,ideal}$ and $T_{mc,max}$ are 176 and 122 °C for PHB, 152 and 100 °C for P34HB-7%, and 156 and 100 °C for P34HB-9% (Figures S6-S8). The nucleating efficiency (NE) of thymine can be quantified using Equation 2 [50]:

$$\mathrm{NE} = 100\ \% \cdot \frac{T_{\mathrm{mc,NA}} - T_{\mathrm{mc,I}}}{T_{\mathrm{mc,max}} - T_{\mathrm{mc,I}}} \quad (2)$$

In Equation 2, $T_{mc,I}$ and $T_{mc,NA}$ represent the melt-crystallization temperatures of the reference and thymine-nucleated film, respectively, measured after erasing the melt memory at 200 °C for 3 min (DI). These values were determined using the DSC non-isothermal crystallization protocol with cooling at 10 K/min (Table 3). The NE of 1 wt% thymine for PHB was calculated to be 44 %. In contrast to the findings reported by Ma et al. [10], the nucleating efficiency of 1 wt% thymine did not exceed that of self-nucleation. In other words, 1 wt% thymine did not exhibit a supernucleation effect for PHB in this study. For the P(3HB-*co*-4HB) samples, $T_{mc,I}$ could not be determined due to the presence of cold-crystallization in DI. Therefore, the nucleation capacity could not be quantified using Equation 2. However, $T_{mc,NA}$ values were equal to 91, 68, and 66 °C for P34HB-6%, P34HB-7%, and P34HB-9%, respectively (Table 3), which did not surpass $T_{mc,max}$, equal to 107, 100, and 100 °C, respectively. Therefore, no supernucleation effect of 1 wt% thymine was observed for the P(3HB-*co*-4HB) samples.

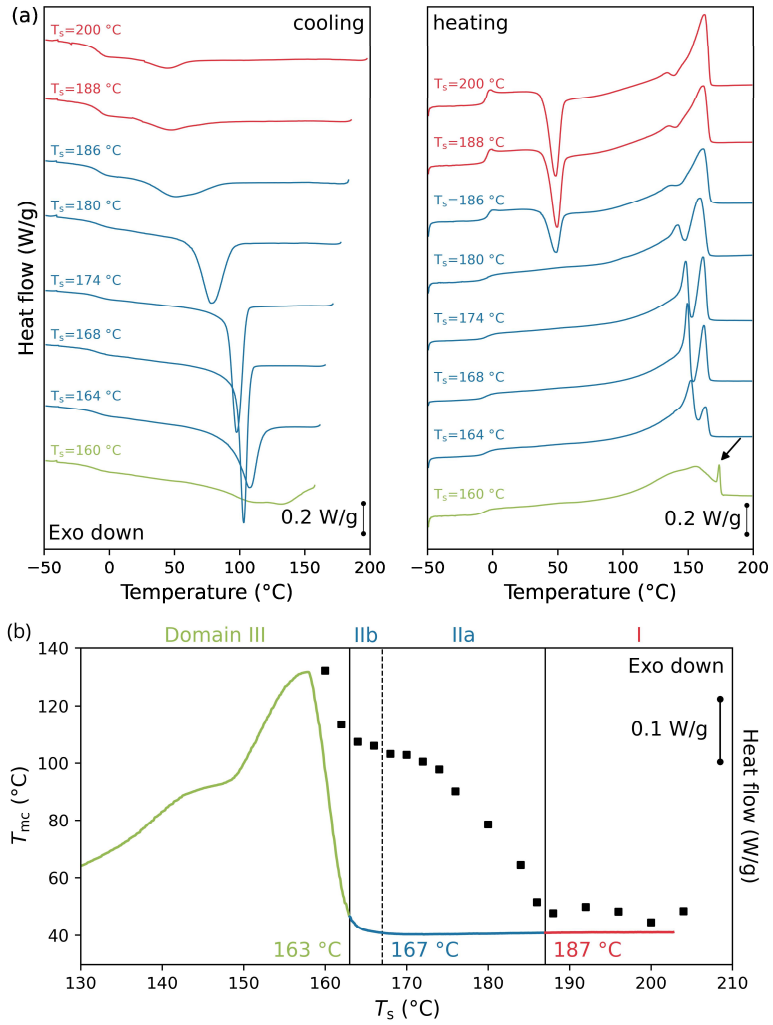

Figure 4. Self-nucleation of P34HB-6% by DSC: (a) Cooling (10 K/min) and subsequent heating curves for selected self-nucleation temperatures (T_s); (b) Melt-crystallization temperatures (T_{mc}, left y-axis) as function of T_s, with the melting endotherm from the first heating overlaid (right y-axis). Self-nucleation domains are indicated. In (a), a black arrow marks the additional high-temperature melting peak, characteristic of annealing in domain III.

The thermal decomposition of PHB, P34HB-6%, P34HB-7%, and P34HB-9%, as well as their mixtures with 1 wt% thymine, was investigated by thermogravimetric analysis (TGA). Results are discussed in Supporting Information (Section S.5). Weight loss for PHB and P(3HB-*co*-4HB) began slightly above 200 °C, and occurred at similar or slightly lower temperatures for the thymine-nucleated samples. In contrast to the observations by Ma et al.

[10], no evidence was found for thymine functioning as a flame retardant. Although efforts were made to minimize thermal degradation during the self-nucleation study, the potential impact of thermal degradation - particularly through a reduction in molar mass - on crystallization cannot be entirely ruled out. However, this is considered beyond the scope of the current research and is not expected to affect the conclusion that thymine does not exhibit a supernucleation effect for the studied PHB and P(3HB-*co*-4HB) materials.

3.6 Effect of thymine on the isothermal crystallization of PHB and P(3HB-co-4HB)

The isothermal melt-crystallization of PHB, P34HB-6%, P34HB-7%, P34HB-9%, and their mixtures with 1 wt% thymine at different crystallization temperatures was investigated using DSC. The protocol includes a fast cooling step from the melt, followed by an isothermal step at the temperature of interest (T_c). The transition between these steps generates a transient overshoot, which may partially overlap with the initial stages of crystallization. To separate the transient overshoot from the crystallization exotherm, Righetti et al. [61] suggested subtracting a blank run from the signal. This blank run should be recorded after isothermal crystallization, using the same sample at a temperature above the melting point, where no phase transformation occurs. However, the blank run exhibited a baseline drift for all studied PHB and P(3HB-*co*-4HB) materials, which is likely due to thermal degradation of the material at these elevated temperatures (Supporting Information, Section S.5). Therefore, a new blank run was recorded at 170 °C, as no phase transition occurs at this temperature (within a 30-minute time span). For each PHB or P(3HB-*co*-4HB) material studied, two blank runs were performed—one on the reference film and one on the 1 wt% thymine-nucleated film. After subtraction of the blank run from the crystallization exotherm, the onset time of crystallization (τ_0) was determined as the last time point where the heat flow rate is zero before the isothermal crystallization peak. The resulting crystallization exotherms (after blank run subtraction and starting from τ_0) are shown

in Figure S10 (Supporting Information). The relative crystallinity X_{rel} at time t, measured from τ_0, was then calculated using Equation 3:

$$X_{\mathrm{rel}}(t) = \int_0^t \frac{dH(t)}{dt} dt / \int_0^\infty \frac{dH(t)}{dt} dt \quad (3)$$

In this equation, $dH(t)/dt$ represents the heat flow rate at time t. The crystallization half-time ($\tau_{0.5}$) was determined as the time, measured from τ_0, where X_{rel} reached 0.5. The resulting $\tau_{0.5}$ values are plotted as function of T_c in Figure 5.

Notably, the crystallization exotherms of the reference samples measured at relatively high T_c (i.e., under low supercooling) were irregularly shaped (Supporting Information, Figure S10). This was particularly the case for the P(3HB-*co*-4HB) reference samples, specifically P34HB-6% at T_c = 90 °C, and P34HB-7% and P34HB-9% at T_c = 80 °C. As described by Di Lorenzo et al. [62], this irregularity can be attributed to the formation of a relatively small number of large spherulites. This likely results from the high purity of PHA polymers (low density of heterogeneous nuclei), combined with a very low homogeneous nucleation rate at low supercooling. To account for these irregular crystallization signals, the $\tau_{0.5}$ values under these conditions were averaged from two independent runs (Figure 5).

Incorporating 4HB as a comonomer into the PHB polymer backbone results in a pronounced shift of the crystallization temperatures to lower values, consistent with the role of 4HB units as structural defects (Supporting Information, Figure S10). Accordingly, considering the P(3HB-*co*-4HB) copolymers, $\tau_{0.5}$ at a given T_c was found to increase with increasing 4HB content (Figure 5). For instance, at T_c = 75 °C, $\tau_{0.5}$ increased from 7 min for P34HB-6% to 17 min for P34HB7%, and further to 22 min for P34HB-9%. Regarding the effect of thymine, a notable reduction in $\tau_{0.5}$ was observed for PHB/TM1 compared to the neat PHB sample. An even more pronounced effect was seen for the P(3HB-*co*-4HB) copolymers: the temperature range in which isothermal crystallization could be observed by DSC shifted significantly toward higher temperatures after mixing with thymine. These findings demonstrate that

addition of 1 wt% thymine greatly enhances the isothermal crystallization rate of PHB and P(3HB-*co*-4HB) with 6-9 mol% 4HB.

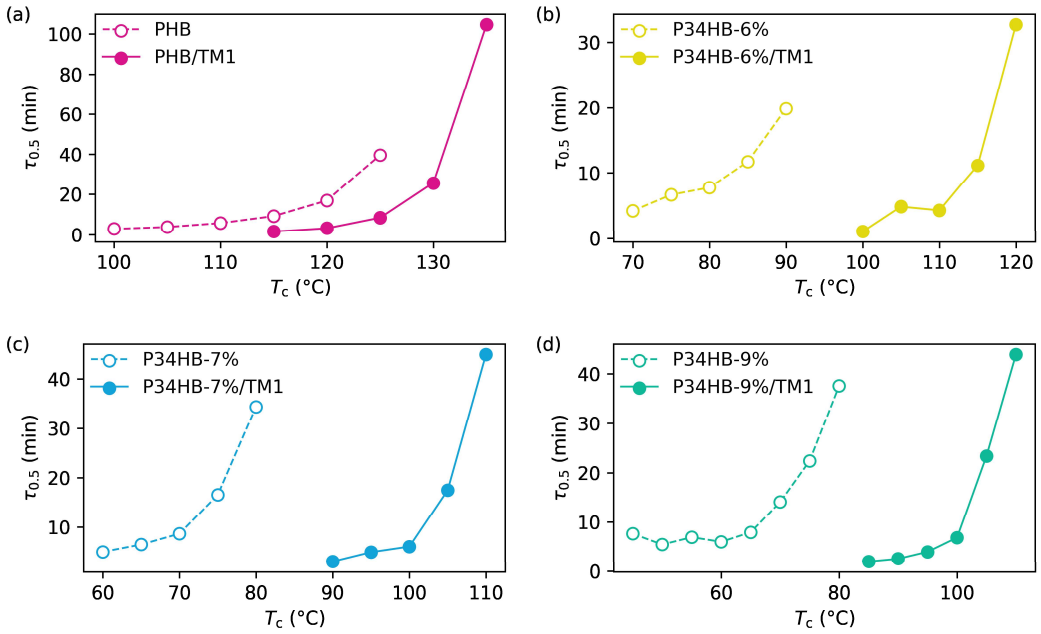

Figure 5. Crystallization half-time ($\tau_{0.5}$) as function of isothermal crystallization temperature (T_c) determined by DSC for (a) PHB, (b) P34HB-6%, (c) P34HB-7%, and (d) P34HB-9%, and their mixtures with 1 wt% thymine.

To further analyze the crystallization kinetics, the Avrami equation was applied [63–65]. These, discussed in Supporting Information (Section S.6), confirm the substantial increase in overall isothermal crystallization rate upon thymine addition.

While a significant enhancement in crystallization rate was observed with thymine, crystallization is governed by both nucleation and crystal growth processes. To assess whether thymine also influences the spherulite growth rate, polarized optical microscopy (POM) was performed at the same T_c each PHB or P(3HB-*co*-4HB) polymer, and its corresponding mixture with 1 wt% thymine. The results, summarized in Table S6 (Supporting Information), showed no significant difference in average spherulite growth rate between reference and thymine-

nucleated samples. This confirms that the observed increase in crystallization rate can be fully attributed to enhanced nucleation density induced by thymine.

3.7 Effect of thymine on mechanical properties of heat-pressed PHB and P(3HB-co-4HB) films

The mechanical properties of PHB and P(3HB-*co*-4HB) films were evaluated to assess the effect of thymine-induced nucleation (1 wt%). Tensile testing was performed on both solvent-cast and heat-pressed samples after 14 days of aging. Results for the solvent-cast samples are discussed in the Supporting Information (Section S.7), while this section focuses on the heat-pressed films. Average mechanical properties are summarized in Table 4, and corresponding POM images are shown in Figure 6. It is important to note that some specimens fractured at or near the clamps but were still included in the dataset. This may have influenced the accuracy of the results. Therefore, while the observed trends offer valuable insights, the mechanical data should be interpreted with caution.

Compared to PHB, the P(3HB-*co*-4HB) copolymers exhibited significantly lower elastic modulus and tensile strength, accompanied by a marked increase in elongation at break. These trends align with the decreased crystallinity associated with 4HB incorporation, as observed by DSC (Section 3.2) and described in literature. The 4HB unit disrupts the regular packing of PHB chains, leading to weaker intermolecular interactions and a reduced crystallinity, which in turn decreases stiffness and strength, while enhancing ductility [6,35,66].

As shown in Table 4, the addition of thymine led to a slight increase in elongation at break across all tested PHB and P(3HB-*co*-4HB) materials. POM analysis (Figure 6) revealed that thymine induced the formation of more uniform and smaller spherulites in the heat-pressed films. However, DSC data (Table 3) confirmed that the overall crystallinity remained largely unchanged. In semi-crystalline polymers, larger spherulites are known to contain numerous

defects (cracks) at their boundaries, which is a common site for fracture under tensile stress. Easier crack propagation at these boundaries typically leads to a reduced elongation at break with increasing spherulite size [67]. Additionally, a slight decrease in elastic modulus and tensile strength was observed for PHB, P34HB-7%, and P34HB-9% upon thymine addition, while P34HB-6% showed a minor increase (Table 4). As discussed in Section 3.5, thymine promotes faster crystallization during cooling - at higher temperatures - resulting in smaller spherulites exhibiting less-defined birefringence patterns, and more pronounced interspherulitic amorphous regions (Figure 6). Although this could influence mechanical performance, most of the observed changes in elastic modulus and tensile strength fell within one standard deviation, suggesting that they may be attributed to experimental variability. These findings highlight the need for further investigation, including studies on bulk materials, as the present results are based on thin (~0.1 mm) films.

Table 4. Mechanical properties of heat-pressed PHB, P34HB-6%, P34HB-7%, P34HB-9%, and their mixtures with 1 wt% thymine, after 14 days of aging. Values are reported as mean ± standard deviation from five replicates.

Sample	Elastic modulus (MPa)	Tensile strength (MPa)	Elongation at break (%)
PHB	$(1.99 \pm 0.30) \times 10^3$	28.8 ± 1.9	2.0 ± 0.4
PHB/TM1	$(1.88 \pm 0.26) \times 10^3$	24.8 ± 1.7	3.8 ± 0.3
P34HB-6%	$(1.12 \pm 0.16) \times 10^3$	17.2 ± 2.4	2.9 ± 0.4
P34HB-6%/TM1	$(1.14 \pm 0.07) \times 10^3$	19.5 ± 1.8	5.5 ± 2.3
P34HB-7%	$(1.17 \pm 0.08) \times 10^3$	20.2 ± 0.8	4.2 ± 0.8
P34HB-7%/TM1	$(9.29 \pm 1.11) \times 10^2$	18.4 ± 2.5	5.2 ± 0.9
P34HB-9%	$(9.02 \pm 1.02) \times 10^2$	16.5 ± 2.3	4.1 ± 1.1
P34HB-9%/TM1	$(7.23 \pm 0.39) \times 10^2$	14.6 ± 3.4	6.0 ± 1.4

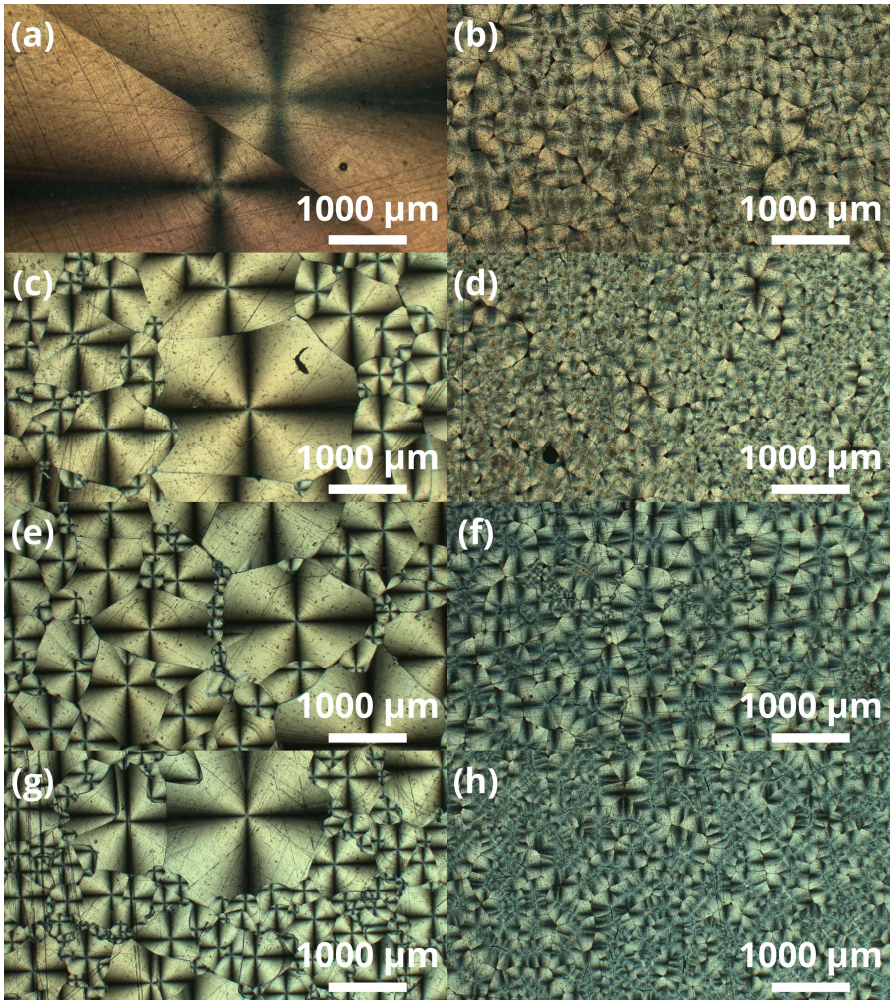

Figure 6. Polarized optical microscopy (POM) images of heat-pressed films of (a) PHB, (b) PHB/TM1, (c) P34HB-6%, (d) P34HB-6%/TM1, (e) P34HB-7%, (f) P34HB-7%/TM1, (g) P34HB-9%, and (h) P34HB-9%/TM1.

4. Conclusion

In this study, PHB and P(3HB-*co*-4HB) copolymers containing 6, 7, and 9 mol% 4HB were biosynthesized through cultivation of *Cupriavidus* sp. USMAA2-4 on various carbon sources. This in-house biosynthesis yielded high-purity materials, enabling a reliable evaluation of thymine - a biobased, biocompatible compound - as a potential nucleating agent.

This is the first report demonstrating that thymine (partially) dissolves in the polymer melt and recrystallizes during cooling into needle-like structures that act as efficient nucleation sites.

Varying the thymine content (0.5–2 wt%) revealed that 1 wt% provided the most reliable and effective enhancement of crystallization. The addition of 1 wt% thymine consistently accelerated crystallization under both non-isothermal and isothermal conditions across all PHB and P(3HB-*co*-4HB) materials, without significantly affecting spherulite growth rates or final crystallinity. Thymine-induced nucleation led to the formation of smaller, more uniformly distributed spherulites, resulting in a modest yet consistent improvement in ductility of thin heat-pressed films.

Despite these benefits, thymine did not display a supernucleation effect, as its nucleating efficiency in this study remained below that of self-nucleation. Notably, this study is the first to report the self-nucleation temperature domains of P(3HB-*co*-4HB) copolymers, providing valuable insights into their crystallization behavior. The nucleating efficiency of melt-soluble organic compounds such as thymine strongly depends on the surface-to-volume ratio of their recrystallized forms, which is influenced by, among others, cooling rate and dispersion quality. Future work should focus on analyzing melt-mixed samples with varying thymine concentrations under a broader range of cooling regimes, particularly at rates representative of industrial processing. Together, these next steps will be essential to fully harness thymine's potential as a melt-soluble nucleating agent for improving both the processability and mechanical performance of PHA-based materials.

ASSOCIATED CONTENT

Data Availability Statement

The data that support the findings of this study are openly available in Zenodo at 10.5281/zenodo.11119380.

Supporting Information

Representative ^{1}H NMR spectrum and PHA dispersity values determined by SEC-MALS, additional DSC crystallization parameters and thermograms, additional POM images of thymine dissolution-recrystallization, additional DSC self-nucleation plots, TGA data and discussion, isothermal crystallization exotherms, modeling of isothermal crystallization data by Avrami equation, spherulite growth rates, and tensile testing of solvent-cast samples (PDF)

AUTHOR INFORMATION

Corresponding author

* Email address: Niko.Van.den.Brande@vub.be

Author contributions

Hannelore Geeraert: conceptualization, formal analysis, funding acquisition, investigation, validation, visualization, and writing. Milan Den Haese: investigation and writing – review & editing. Louis Pitet: resources and writing – review & editing. Eveline Peeters: funding acquisition, resources, supervision, and writing – review & editing. Niko Van den Brande: conceptualization, funding acquisition, resources, supervision, and writing – review & editing.

Funding sources

This work was financially supported by Research Foundation Flanders (FWO-Vlaanderen) (PhD Fellowship Fundamental Research to Hannelore Geeraert (grant number 11K8423N)), by the Special Research Fund (BOF) of Hasselt University (grant number BOF22KP04), and by the Vrije Universiteit Brussel (Strategic Research Program SRP91).

ACKNOWLEDGEMENTS

The authors would like to thank Prof. Steven Goderis, AMGC, Vrije Universiteit Brussel for access to the polarized optical microscopes. We also gratefully acknowledge Dominika Ośka for her valuable assistance with the experimental work during her internship. The authors acknowledge the use of artificial intelligence (AI) to assist with writing, including improving clarity, refining sentence structure, and correcting grammar and spelling.

REFERENCES

(1) Koller, M.; Mukherjee, A. A New Wave of Industrialization of PHA Biopolyesters. *Bioengineering* **2022**, *9* (2), 74. https://doi.org/10.3390/bioengineering9020074.

(2) Pandey, A.; Adama, N.; Adjallé, K.; Blais, J.-F. Sustainable Applications of Polyhydroxyalkanoates in Various Fields: A Critical Review. *Int J Biol Macromol* **2022**, *221*, 1184–1201. https://doi.org/10.1016/j.ijbiomac.2022.09.098.

(3) Sun, B. X.; Feng, X. Q.; Chuai, C. Z.; Guo, Y.; Luo, S. Effect of the Nucleating Agent BN on Crystallization Properties of P(3HB-Co-4HB). *Adv Mat Res* **2013**, *627*, 827–830. https://doi.org/10.4028/www.scientific.net/AMR.627.827.

(4) Puente, J. A. S.; Esposito, A.; Chivrac, F.; Dargent, E. Effect of Boron Nitride as a Nucleating Agent on the Crystallization of Bacterial Poly(3-hydroxybutyrate). *J Appl Polym Sci* **2013**, *128* (5), 2586–2594. https://doi.org/10.1002/app.38182.

(5) Kai, W.; He, Y.; Inoue, Y. Fast Crystallization of Poly(3-hydroxybutyrate) and Poly(3-hydroxybutyrate-*Co*-3-hydroxyvalerate) with Talc and Boron Nitride as Nucleating Agents. *Polym Int* **2005**, *54* (5), 780–789. https://doi.org/10.1002/pi.1758.

(6) Laycock, B.; Halley, P.; Pratt, S.; Werker, A.; Lant, P. The Chemomechanical Properties of Microbial Polyhydroxyalkanoates. *Prog Polym Sci* **2014**, *39* (2), 397–442. https://doi.org/10.1016/j.progpolymsci.2013.06.008.

(7) Huong, K.-H.; Sevakumaran, V.; Amirul, A. A. P(3HB-*Co*-4HB) as High Value Polyhydroxyalkanoate: Its Development over Recent Decades and Current Advances. *Crit Rev Biotechnol* **2021**, *41* (4), 474–490. https://doi.org/10.1080/07388551.2020.1869685.

(8) Hu, J.; Xia, R.; Yang, H.; Lu, X. Morphology, Mechanical Property, and Modeling Evaluation of P(3HB-co-4HB)/Nano-ZnO Composites. *Polym Compos* **2016**, *37* (10), 3113–3121. https://doi.org/10.1002/pc.23509.

(9) Wang, Q.; Xu, Y.; Xu, P.; Yang, W.; Chen, M.; Dong, W.; Ma, P. Crystallization of Microbial Polyhydroxyalkanoates: A Review. *Int J Biol Macromol* **2022**, *209*, 330–343. https://doi.org/10.1016/j.ijbiomac.2022.04.018.

(10) Ma, H.; Wei, Z.; Zhou, S.; Zhu, H.; Tang, J.; Yin, J.; Yue, J.; Yang, J. Supernucleation, Crystalline Structure and Thermal Stability of Bacterially Synthesized Poly(3-Hydroxybutyrate) Polyester Tailored by Thymine as a Biocompatible Nucleating Agent. *Int J Biol Macromol* **2020**, *165*, 1562–1573. https://doi.org/10.1016/j.ijbiomac.2020.10.044.

(11) Wang, L.; Wang, X.; Zhu, W.; Chen, Z.; Pan, J.; Xu, K. Effect of Nucleation Agents on the Crystallization of Poly(3-hydroxybutyrate- *Co* -4-hydroxybutyrate) (P3/4HB). *J Appl Polym Sci* **2010**, *116* (2), 1116–1123. https://doi.org/10.1002/app.31588.

(12) Han, L.; Han, C.; Cao, W.; Wang, X.; Bian, J.; Dong, L. Preparation and Characterization of Biodegradable Poly(3-hydroxybutyrate-*Co*-4-hydroxybutyrate)/Silica Nanocomposites. *Polym Eng Sci* **2012**, *52* (2), 250–258. https://doi.org/10.1002/pen.22076.

(13) Yu, Y.; Li, Y.; Han, C.; Xiao, L. Enhancement of the Properties of Biosourced Poly(3-Hydroxybutyrate-Co-4-Hydroxybutyrate) by the Incorporation of Natural Orotic Acid. *Int J Biol Macromol* **2019**, *136*, 764–773. https://doi.org/10.1016/j.ijbiomac.2019.06.056.

(14) Che, X.-M.; Ye, H.-M.; Chen, G.-Q. Effects of Uracil on Crystallization and Rheological Property of Poly(R-3-Hydroxybutyrate-Co-4-Hydroxybutyrate). *Compos Part A Appl Sci Manuf* **2018**, *109*, 141–150. https://doi.org/10.1016/j.compositesa.2018.03.006.

(15) Gao, P.; Masato, D. The Effects of Nucleating Agents and Processing on the Crystallization and Mechanical Properties of Polylactic Acid: A Review. *Micromachines (Basel)* **2024**, *15* (6), 776. https://doi.org/10.3390/mi15060776.

(16) Li, H.; Lu, X.; Yang, H.; Hu, J. Non-Isothermal Crystallization of P(3HB-Co-4HB)/PLA Blends. *J Therm Anal Calorim* **2015**, *122* (2), 817–829. https://doi.org/10.1007/s10973-015-4824-5.

(17) Qian, J.; Zhu, L.; Zhang, J.; Whitehouse, R. S. Comparison of Different Nucleating Agents on Crystallization of Poly(3-hydroxybutyrate- *Co* -3-hydroxyvalerates). *J Polym Sci B Polym Phys* **2007**, *45* (13), 1564–1577. https://doi.org/10.1002/polb.21157.

(18) Pan, P.; Liang, Z.; Nakamura, N.; Miyagawa, T.; Inoue, Y. Uracil as Nucleating Agent for Bacterial Poly[(3-Hydroxybutyrate)-Co-(3-Hydroxyhexanoate)] Copolymers. *Macromol Biosci* **2009**, *9* (6), 585–595. https://doi.org/10.1002/mabi.200800294.

(19) Sangroniz, L.; Cavallo, D.; Müller, A. J. Self-Nucleation Effects on Polymer Crystallization. *Macromolecules* **2020**, *53* (12), 4581–4604. https://doi.org/10.1021/acs.macromol.0c00223.

(20) Hu, W. Polymer Crystallization. In *Polymer Physics*; Springer Vienna: Vienna, 2012; pp 187–221. https://doi.org/10.1007/978-3-7091-0670-9_10.

(21) Aliotta, L.; Sciara, L. M.; Cinelli, P.; Canesi, I.; Lazzeri, A. Improvement of the PLA Crystallinity and Heat Distortion Temperature Optimizing the Content of Nucleating Agents and the Injection Molding Cycle Time. *Polymers (Basel)* **2022**, *14* (5), 977. https://doi.org/10.3390/polym14050977.

(22) Di Lorenzo, M. L.; Sajkiewicz, P.; Gradys, A.; La Pietra, P. Optimization of Melting Conditions for the Analysis of Crystallization Kinetics of Poly(3-Hydroxybutyrate). *e-Polymers* **2009**, *9* (1), No. 027. https://doi.org/10.1515/epoly.2009.9.1.313.

(23) Xu, P.; Wang, Q.; Yu, M.; Yang, W.; Weng, Y.; Dong, W.; Chen, M.; Wang, Y.; Ma, P. Enhanced Crystallization and Storage Stability of Mechanical Properties of Biosynthesized Poly (3-Hydroxybutyrate-Co-3-Hydroxyhexanate) Induced by Self-Nucleation. *Int J Biol Macromol* **2021**, *184*, 797–803. https://doi.org/10.1016/j.ijbiomac.2021.06.120.

(24) Bossu, J.; Le Moigne, N.; Dieudonné-George, P.; Dumazert, L.; Guillard, V.; Angellier-Coussy, H. Impact of the Processing Temperature on the Crystallization

Behavior and Mechanical Properties of Poly[R-3-Hydroxybutyrate-Co-(R-3-Hydroxyvalerate)]. *Polymer (Guildf)* **2021**, *229*, 123987. https://doi.org/10.1016/j.polymer.2021.123987.

(25) Pagliano, G.; Galletti, P.; Samorì, C.; Zaghini, A.; Torri, C. Recovery of Polyhydroxyalkanoates From Single and Mixed Microbial Cultures: A Review. *Front Bioeng Biotechnol* **2021**, *9*, 624021. https://doi.org/10.3389/fbioe.2021.624021.

(26) Doineau, E.; Perdrier, C.; Allayaud, F.; Blanchet, E.; Preziosi-belloy, L.; Grousseau, E.; Gontard, N.; Angellier-Coussy, H. Designing Poly(3-Hydroxybutyrate-Co-3-Hydroxyvalerate) P(3HB-Co-3HV) Films with Tailored Mechanical Properties. *Mater Today Commun* **2023**, *36*, 106848. https://doi.org/10.1016/j.mtcomm.2023.106848.

(27) *The Handbook of Polyhydroxyalkanoates, Three Volume Set*; Koller, M., Ed.; CRC Press, 2020. https://doi.org/10.1201/9781003080718.

(28) Md. Iqbal, N.; Amirul, A. A. Synthesis of P(3HB-co-4HB) Copolymer with Target-specific 4HB Molar Fractions Using Combinations of Carbon Substrates. *Journal of Chemical Technology & Biotechnology* **2014**, *89* (3), 407–418. https://doi.org/10.1002/jctb.4133.

(29) Barham, P. J.; Keller, A.; Otun, E. L.; Holmes, P. A. Crystallization and Morphology of a Bacterial Thermoplastic: Poly-3-Hydroxybutyrate. *J Mater Sci* **1984**, *19* (9), 2781–2794. https://doi.org/10.1007/BF01026954.

(30) Vigneswari, S.; Vijaya, S.; Majid, M. I. A.; Sudesh, K.; Sipaut, C. S.; Azizan, M. N. M.; Amirul, A. A. Enhanced Production of Poly(3-Hydroxybutyrate-Co-4-Hydroxybutyrate) Copolymer with Manipulated Variables and Its Properties. *J Ind*

Microbiol Biotechnol **2009**, *36* (4), 547–556. https://doi.org/10.1007/s10295-009-0525-z.

(31) Tsuge, T. Fundamental Factors Determining the Molecular Weight of Polyhydroxyalkanoate during Biosynthesis. *Polym J* **2016**, *48* (11), 1051–1057. https://doi.org/10.1038/pj.2016.78.

(32) Prieto, A.; Escapa, I. F.; Martínez, V.; Dinjaski, N.; Herencias, C.; de la Peña, F.; Tarazona, N.; Revelles, O. A Holistic View of Polyhydroxyalkanoate Metabolism in *Pseudomonas Putida*. *Environ Microbiol* **2016**, *18* (2), 341–357. https://doi.org/10.1111/1462-2920.12760.

(33) Feng, L.; Watanabe, T.; Wang, Y.; Kichise, T.; Fukuchi, T.; Chen, G.-Q.; Doi, Y.; Inoue, Y. Studies on Comonomer Compositional Distribution of Bacterial Poly(3-Hydroxybutyrate-*Co*-3-Hydroxyhexanoate)s and Thermal Characteristics of Their Factions. *Biomacromolecules* **2002**, *3* (5), 1071–1077. https://doi.org/10.1021/bm0200581.

(34) Van Krevelen, D. W.; Te Nijenhuis, K. Transition Temperatures. In *Properties of Polymers*; Elsevier, 2009; pp 129–188. https://doi.org/10.1016/B978-0-08-054819-7.00006-6.

(35) Wen, X.; Lu, X.; Peng, Q.; Zhu, F.; Zheng, N. Crystallization Behaviors and Morphology of Biodegradable Poly(3-Hydroxybutyrate-Co-4-Hydroxybutyrate). *J Therm Anal Calorim* **2012**, *109* (2), 959–966. https://doi.org/10.1007/s10973-011-1768-2.

(36) Righetti, M. C.; Di Lorenzo, M. L. Melting Temperature Evolution of Non-Reorganized Crystals. Poly(3-Hydroxybutyrate). *Thermochim Acta* **2011**, *512* (1), 59–66. https://doi.org/10.1016/j.tca.2010.08.023.

(37) Tong, B.-B.; Ding, Y.-H. Crystallization Kinetics and Multiple Melting Behavior of Biodegradable Poly(3-Hydroxybutyrate-Co-4-Hydroxybutyrate). *International Polymer Processing* **2018**, *33* (5), 669–676. https://doi.org/10.3139/217.3599.

(38) Mitomo, H.; Hsieh, W.-C.; Nishiwaki, K.; Kasuya, K.; Doi, Y. Poly(3-Hydroxybutyrate-Co-4-Hydroxybutyrate) Produced by Comamonas Acidovorans. *Polymer (Guildf)* **2001**, *42* (8), 3455–3461. https://doi.org/10.1016/S0032-3861(00)00678-9.

(39) Lu, X.; Wen, X.; Yang, D. Isothermal Crystallization Kinetics and Morphology of Biodegradable Poly(3-Hydroxybutyrate-Co-4-Hydroxybutyrate). *J Mater Sci* **2011**, *46* (5), 1281–1288. https://doi.org/10.1007/s10853-010-4912-7.

(40) Wypych, A.; Wypych, G. Others. In *Databook of Nucleating Agents*; Elsevier, 2016; pp 353–368. https://doi.org/10.1016/B978-1-895198-94-2.50018-7.

(41) Ma, H.; Wei, Z.; Zhou, S.; Zhu, H.; Tang, J.; Yin, J.; Yue, J.; Yang, J. Supernucleation, Crystalline Structure and Thermal Stability of Bacterially Synthesized Poly(3-Hydroxybutyrate) Polyester Tailored by Thymine as a Biocompatible Nucleating Agent. *Int J Biol Macromol* **2020**, *165*, 1562–1573. https://doi.org/10.1016/j.ijbiomac.2020.10.044.

(42) Ma, P.; Deshmukh, Y. S.; Wilsens, C. H. R. M.; Ryan Hansen, M.; Graf, R.; Rastogi, S. Self-Assembling Process of Oxalamide Compounds and Their Nucleation

Efficiency in Bio-Degradable Poly(Hydroxyalkanoate)s. *Sci Rep* **2015**, *5* (1), 13280. https://doi.org/10.1038/srep13280.

(43) Shen, T.; Xu, Y.; Cai, X.; Ma, P.; Dong, W.; Chen, M. Enhanced Crystallization Kinetics of Poly(Lactide) with Oxalamide Compounds as Nucleators: Effect of Spacer Length between the Oxalamide Moieties. *RSC Adv* **2016**, *6* (54), 48365–48374. https://doi.org/10.1039/C6RA04050K.

(44) Horváth, F.; Bihari, L.; Bodrogi, D.; Gombár, T.; Hilt, B.; Keszei, B.; Krain, T.; Simon, A.; Menyhárd, A. Effect of *N* , *N* ′-Dicyclohexyldicarboxamide Homologues on the Crystallization and Properties of Isotactic Polypropylene. *ACS Omega* **2021**, *6* (13), 9053–9065. https://doi.org/10.1021/acsomega.1c00064.

(45) Seven, K. M.; Cogen, J. M.; Gilchrist, J. F. Nucleating Agents for High-Density Polyethylene - A Review. *Polym Eng Sci* **2016**, *56* (5), 541–554. https://doi.org/10.1002/pen.24278.

(46) Leoné, N.; Roy, M.; Saidi, S.; de Kort, G.; Hermida-Merino, D.; Wilsens, C. H. R. M. Improving Processing, Crystallization, and Performance of Poly-L-Lactide with an Amide-Based Organic Compound as Both Plasticizer and Nucleating Agent. *ACS Omega* **2019**, *4* (6), 10376–10387. https://doi.org/10.1021/acsomega.9b00848.

(47) Kristiansen, M.; Werner, M.; Tervoort, T.; Smith, P.; Blomenhofer, M.; Schmidt, H.-W. The Binary System Isotactic Polypropylene/Bis(3,4-Dimethylbenzylidene)Sorbitol: Phase Behavior, Nucleation, and Optical Properties. *Macromolecules* **2003**, *36* (14), 5150–5156. https://doi.org/10.1021/ma030146t.

(48) Fan, Y.; Yan, S.; Yin, J. The Relationship between Solubility and Nucleating Effect of Organic Nucleating Agent in Poly(L-lactic Acid). *J Appl Polym Sci* **2019**, *136* (7), 46851. https://doi.org/10.1002/app.46851.

(49) Luo, F.; Geng, C.; Wang, K.; Deng, H.; Chen, F.; Fu, Q.; Na, B. New Understanding in Tuning Toughness of β-Polypropylene: The Role of β-Nucleated Crystalline Morphology. *Macromolecules* **2009**, *42* (23), 9325–9331. https://doi.org/10.1021/ma901651f.

(50) Fillon, B.; Lotz, B.; Thierry, A.; Wittmann, J. C. Self-nucleation and Enhanced Nucleation of Polymers. Definition of a Convenient Calorimetric "Efficiency Scale" and Evaluation of Nucleating Additives in Isotactic Polypropylene (α Phase). *J Polym Sci B Polym Phys* **1993**, *31* (10), 1395–1405. https://doi.org/10.1002/polb.1993.090311014.

(51) Michell, R. M.; Mugica, A.; Zubitur, M.; Muller, A. J. Self-Nucleation of Crystalline Phases within Homopolymers, Polymer Blends, Copolymers, and Nanocomposites. *Advances in Polymer Science* **2017**, *276*, 215–256. https://doi.org/10.1007/12_2015_327.

(52) Alizadehaghdam, M.; Abbasi, F.; Reiter, G. Successive Melting and Crystallization of Poly(3-Hexylthiophene) in the Melt-Memory Domain versus Isotropic Melt Domain. *J Mater Sci* **2021**, *56* (35), 19723–19737. https://doi.org/10.1007/s10853-021-06594-7.

(53) Thomas, D.; Cebe, P. Self-Nucleation and Crystallization of Polyvinyl Alcohol. *J Therm Anal Calorim* **2017**, *127* (1), 885–894. https://doi.org/10.1007/s10973-016-5811-1.

(54) Hu, S.; Yang, F.; Xiang, M.; Cao, Y.; Wu, T.; Fu, Q. Competition of Memory Effect and Thermal Degradation on the Crystallization Behavior of Polyphenylene Sulfide. *Polymer (Guildf)* **2022**, *262*. https://doi.org/10.1016/j.polymer.2022.125427.

(55) Shang, Y. The Melt Memory Effects in Polymer Crystallization. *Journal of Polymer Science* **2024**, *62* (11), 2340–2354. https://doi.org/10.1002/pol.20230882.

(56) Jiang, J.; Zhuravlev, E.; Hu, W.; Schick, C.; Zhou, D. The Effect of Self-Nucleation on Isothermal Crystallization Kinetics of Poly(Butylene Succinate) (PBS) Investigated by Differential Fast Scanning Calorimetry. *Chinese Journal of Polymer Science* **2017**, *35* (8), 1009–1019. https://doi.org/10.1007/s10118-017-1942-5.

(57) Wei, Z.; Qv, C.; Li, W.; Zhao, R.; Ma, Z. Influence of Self-Nucleation on Phase Transition in Poly(1-Butene). *Polymer (Guildf)* **2023**, *272*, 125846. https://doi.org/10.1016/j.polymer.2023.125846.

(58) Hu, D.; Ye, S.; Yu, F.; Feng, J. Further Understanding on the Three Domains of Isotactic Polypropylene by Investigating the Crystalline Morphologies Evolution after Treatment at Different Domains. *Chinese Journal of Polymer Science* **2016**, *34* (3), 344–358. https://doi.org/10.1007/s10118-016-1745-0.

(59) Fillon, B.; Wittmann, J. C.; Lotz, B.; Thierry, A. Self-nucleation and Recrystallization of Isotactic Polypropylene (α Phase) Investigated by Differential Scanning Calorimetry. *J Polym Sci B Polym Phys* **1993**, *31* (10), 1383–1393. https://doi.org/10.1002/polb.1993.090311013.

(60) Trujillo, M.; Arnal, M. L.; Müller, A. J.; Mujica, M. A.; Urbina de Navarro, C.; Ruelle, B.; Dubois, P. Supernucleation and Crystallization Regime Change Provoked by

MWNT Addition to Poly(ε-Caprolactone). *Polymer (Guildf)* **2012**, *53* (3), 832–841. https://doi.org/10.1016/j.polymer.2011.12.028.

(61) Righetti, M. C.; Di Lorenzo, M. L.; Angiuli, M.; Tombari, E.; La Pietra, P. Poly(Butylene Terephthalate)/Poly(ε-Caprolactone) Blends: Influence of PCL Molecular Mass on PBT Melting and Crystallization Behavior. *Eur Polym J* **2007**, *43* (11), 4726–4738. https://doi.org/10.1016/j.eurpolymj.2007.08.020.

(62) Di Lorenzo, M. L.; Sajkiewicz, P.; La Pietra, P.; Gradys, A. Irregularly Shaped DSC Exotherms in the Analysis of Polymer Crystallization. *Polymer Bulletin* **2006**, *57* (5), 713–721. https://doi.org/10.1007/s00289-006-0621-4.

(63) Avrami, M. Kinetics of Phase Change. I General Theory. *J Chem Phys* **1939**, *7* (12), 1103–1112. https://doi.org/10.1063/1.1750380.

(64) Avrami, M. Kinetics of Phase Change. II Transformation-Time Relations for Random Distribution of Nuclei. *J Chem Phys* **1940**, *8* (2), 212–224. https://doi.org/10.1063/1.1750631.

(65) Avrami, M. Granulation, Phase Change, and Microstructure Kinetics of Phase Change. III. *J Chem Phys* **1941**, *9* (2), 177–184. https://doi.org/10.1063/1.1750872.

(66) Jo, M.; Jang, Y.; Lee, E.; Shin, S.; Kang, H. The Modification of Poly(3-Hydroxybutyrate-Co-4-Hydroxybutyrate) by Melt Blending. *Polymers (Basel)* **2022**, *14* (9), 1725. https://doi.org/10.3390/polym14091725.

(67) Pavlov, V. I. Investigation of the Effect of Spherulite Size on the Strength and Deformation Characteristics of Isotactic Polypropylene Films. *Soviet Materials Science* **1971**, *4* (5), 438–440. https://doi.org/10.1007/BF00721450.